Modulating the Reactivity of Liquid Ga Nanoparticles by Modifying their Surface Chemistry

Laia Castilla-Amorós†, Tzu-Chin Chang Chien†, James R. Pankhurst†, Raffaella Buonsanti†*

† Laboratory of Nanochemistry for Energy (LNCE), Institute of Chemical Sciences and Engineering, École Polytechnique Fédérale de Lausanne, CH-1950 Sion, Switzerland.

ABSTRACT

Micron- and nano-sized particles of liquid metals, particularly Ga-based alloys, are attracting increasing attention for applications in several fields. Their native oxide skin regulates many of their properties; yet, very little is known about its chemistry. Here, we investigate the impact of selected capping ligands on the native oxide thickness of Ga nanoparticles (NPs) and on their chemical reactivity, choosing the galvanic replacement reaction (GRR) as one example. We demonstrate that amines and carboxylic acids promote thicker oxide shells while thiols and phosphines hinder the oxide growth. Upon pondering thermodynamics and kinetics factors, we conclude the affinity of the anchoring group towards the metal core being the major driver. We go on to prove that thicker shells foster the formation of Cu-Ga nanodimers following the reaction of the Ga NPs with a copper amine complex. In contrast, thinner oxides lead to the homogeneous nucleation of individual Cu NPs. This study reveals the importance of the choice of ligand when studying Ga-based metal NPs for different applications since both their surface chemistry and reactivity are largely affected by this decision.

INTRODUCTION

Liquid metals (LMs) are a class of materials that is attracting a renewed interest thanks to their fascinating properties arising from their simultaneous metallic and liquid nature.[1–3] Among all possible compositions, most research focuses on metallic Ga and its alloys because of their low melting temperatures and their unique electrical and rheological characteristics.[4] The latter open up new possibilities in various fields, including electronics, microfluidics, biomedicine, batteries, as well as for synthetic and catalytic applications.[5–14]

So far, most of the work has centered on bulk and micron-sized particles. Nevertheless, new physicochemical properties emerge when the size of Ga-based particles shrinks down to the nanoscale.[3] For example, plasmonic and catalytic properties can be modulated with the size of the particles and are influenced by their size-dependent solid-liquid transition.[11,14,15] In addition to the chemical composition of the bulk, the native oxide skin of Ga-based particles plays a crucial role in determining their chemical and mechanical behavior.[4,16,17] For instance, the thickness of the surface oxide can modify surface adhesion and wetting properties[18–20] as well as tuning the on/off state in soft electronics[21–23]. As an additional example, it has been recently discovered that a smooth oxide skin can stabilize LM particles in their undercooled state.[24] Interestingly, molecular coatings have been shown to significantly impact the surface properties of Ga-based particles, particularly the thickness and roughness of their oxide skin.[24–27] However, these studies still remain isolated examples and the relationship between the chemical nature of the molecules and their role as surface modifiers has not been thoroughly investigated so far.

Herein, we investigate the impact of capping ligands with different anchoring groups on the surface properties of Ga nanoparticles (NPs). The oxide skin for most of the Ga-based LM

alloys, including galinstan ($Ga_{68.5}In_{21.5}Sn_{10}$), eutectic GaIn and GaPd droplets, is essentially gallium oxide, which is due to its higher absolute Gibbs free energy of formation compared to the oxides of other elements.[3,16,28–30] Hence, pure Ga is an ideal choice to study the generality of the surface properties of these materials. Furthermore, ligand effects observed at the bulk and the micron scales are expected to be even greater at the nanoscale, where the surface-to-volume ratio increases, which justifies the choice of using NPs as our model system. We combine transmission electron microscopy (TEM), elemental analysis and X-Ray photoelectron spectroscopy (XPS) to study the Ga oxide skin in the presence of carboxylic acid, amine, thiol and phosphine ligands. We then correlate the chemical nature of the capping ligands to the skin thickness, taking into account both thermodynamic and kinetic factors. Going one step further, we also investigate how the oxide thickness of the LM NPs modulates their chemical reactivity, taking the galvanic replacement reaction (GRR) with a molecular copper precursor as one example.

EXPERIMENTAL SECTION

Materials and chemicals

Tris(dimethylamido)gallium(III) dimer ($Ga_2(NMe_2)_6$, 99.9%) was purchased from ABCR. Copper(II) acetate ($Cu(OAc)_2$, 99.999%), oleic acid ($C_{17}H_{33}CO_2H$ or OLAC, 90%), 1-octadecene ($C_{18}H_{36}$ or ODE, 90%), oleylamine ($C_{18}H_{35}NH_2$ or OLAM, 70%), dodecanethiol ($C_{12}H_{25}SH$ or DDT, 98%), ethanol (anhydrous, 95%) and toluene (anhydrous, 99.8%) were all purchased from Sigma-Aldrich. Tri-n-octylphosphine ($C_{24}H_{51}P$ or TOP, 90%) was purchased from Alfa Aesar. ODE, OLAC, OLAM, and DDT were degassed and dried under a vacuum at

110 °C for 4 h, cooled to room temperature, and then transferred to the glove box. All syntheses were carried out under an inert atmosphere using anhydrous solvents and standard glovebox and Schlenk-line techniques. Post-synthetic purification ("washing"), ligand exchange, handling, and storage of the as-synthesized materials were also carried out under an inert atmosphere.

Materials Synthesis

Ga NPs with different capping ligands. Ga NPs were synthesized by modifying previously reported procedures.[11,31] In a typical synthesis (**Figure S1**), 7 mL of ODE were loaded into a 25 mL three-necked flask, equipped with a reflux condenser, and dried under vacuum at 110 °C for 1 h. Then the reaction flask was filled with N_2 and heated to 290 °C, followed by a rapid injection of a solution containing 50 mg of $Ga_2(NMe_2)_6$ in 3.75 mL of dried ODE with a 20 mL syringe, which had been previously prepared in a glovebox. Right after the injection, the temperature dropped to 235 – 240 °C and after 30 seconds the solution colour changed from yellow to dark grey, indicating the formation of NPs. The capping ligand of choice (OLAC, OLAM, TOP or DDT) was then injected into the reaction flask with a 50:1 molar ratio to the precursor. The reaction flask was then ~~quenched and~~ rapidly cooled down to room temperature using an ice bath. The Ga NPs were separated from any by-products and from unreacted precursors by adding 15 mL of ethanol, followed by centrifugation at 5000 rpm for 20 min. The Ga NPs were redispersed in toluene, and the purification/precipitation step was repeated one more time with one more addition of 0.1 mL of the chosen ligand. The Ga NPs were finally stored in anhydrous toluene.

Cu-Ga NPs. Cu-Ga NPs were synthesized by adapting a previously reported procedure for Cu-Ga nanodimers.[31] Ga NPs with different capping ligands in toluene were transferred to ODE

to form a 4 mM solution (based on atomic concentration from elemental analysis). Soon after, 1 mL of this new solution, 1 mL of a solution of $Cu(OAc)_2$ in ODE (4 mM), 0.5 mL of OLAC and 0.5 mL of OLAM were added to a 5 mL vial and then stirred at 600 rpm on a hot plate at 150 °C inside a glovebox for 4 h. Cu-Ga NPs were separated from any by-products and from unreacted precursors by adding 3 mL of ethanol, followed by centrifugation at 5000 rpm for 20 min. The final product was then redispersed in toluene, and the purification/precipitation step was repeated once before finally being stored in anhydrous toluene.

Characterization

Electron Microscopy. Transmission electron microscopy (TEM) images were recorded on a FEI Tecnai-Spirit at 120 kV, equipped with a Gatan camera. High-angle annular dark-field scanning TEM (HAADF-STEM) imaging and energy dispersive X-ray spectroscopy (EDX) were performed on a FEI Tecnai-Osiris TEM in scanning mode at an accelerating voltage of 200 kV. The microscope is equipped with a high brightness X-FEG gun, silicon drift Super-X EDXS detectors and Bruker Esprit acquisition software. Samples were drop-cast on either a copper or gold TEM grid (Ted Pella, Inc.) prior to imaging.

Inductively Coupled Plasma – Optical Emission Spectroscopy (ICP-OES). Samples were digested with concentrated HNO_3 and then diluted for analysis. The concentrations of the NP solutions were determined on an Agilent 5110 inductively coupled plasma optical emission spectrometry system with a VistaChip II CCD detector.

X-ray Photoelectron Spectroscopy (XPS). Samples were recorded using an Axis Supra (Kratos Analyical) instrument, using the monochromated K_α X-ray line of an Al anode. The pass energy was set to 40 eV with a step size of 0.15 eV. The samples were electrically insulated from the sample holder and charges were compensated. Ga NP samples were prepared by drop-casting

films onto clean Si substrates inside a N_2-filled glovebox. XPS fitting was carried out in Kratos ESCApe software. All data were referenced to the principal C1s peak at 284.8 eV after fitting and any deconvolution of the C1s peak. In the Ga2p region, only the $Ga2p_{3/2}$ peaks were used for fitting and quantification. In the Ga3d region, both Ga and GaO_x peaks were fitted with contributions from spin-orbit coupling; the $Ga3d_{3/2}$ and $Ga3d_{5/2}$ peak separations were fixed at 0.46 eV and the relative intensities were fixed at 0.633. In both regions, the peaks for elemental gallium were fitted using asymmetric functions. In general, all peaks from a particular region were first fitted with equal linewidths, and then this constraint was relaxed to refine the fit.

RESULTS AND DISCUSSION

Colloidal Ga NPs were synthesized by adapting a previously reported procedure (**Figure S1**).[11] Four different ligands were utilized during the synthesis, specifically oleic acid (OLAC), oleylamine (OLAM), tri-n-octylphosphine (TOP) and dodecanethiol (DDT). These ligands were selected because of the different affinities of their anchoring groups towards metal surfaces. In particular, OLAC and OLAM are known to bind to oxide surfaces more strongly than metallic surfaces, therefore they should stabilize the oxide skin of LM NPs.[25,26,32–35] Conversely, DDT and TOP have a higher affinity to metals, thus they are expected to stabilize the metal core and inhibit the oxide formation.[25,26,32–35] Furthermore, these ligands are all readily available and commonly used in NP synthesis.

Figure 1 gives an overview of the characterization of the as-synthesized samples. In the TEM images (**Figure 1a**), the lack of diffraction contrast, which would denote crystallinity, indicates that all the NPs are amorphous, i.e., liquid, which is consistent with previous reports.[11,31] The size distribution analysis evidences that the different ligands have no major effect on the morphology and final size of the Ga NPs, which are all spherical with a mean size of around 30 nm (**Figure S2)**. Indeed, the ligands were intentionally added to the reaction flask after the NP formation (**Figure S1**) to minimize their impact on the nucleation and growth steps, and thus on size and shape. XPS (**Figure 1b**) evidences that -COOH, -N, -P and -S are on the NP surface, consistent with OLAC, OLAM, TOP and DDT being the capping agents, respectively.

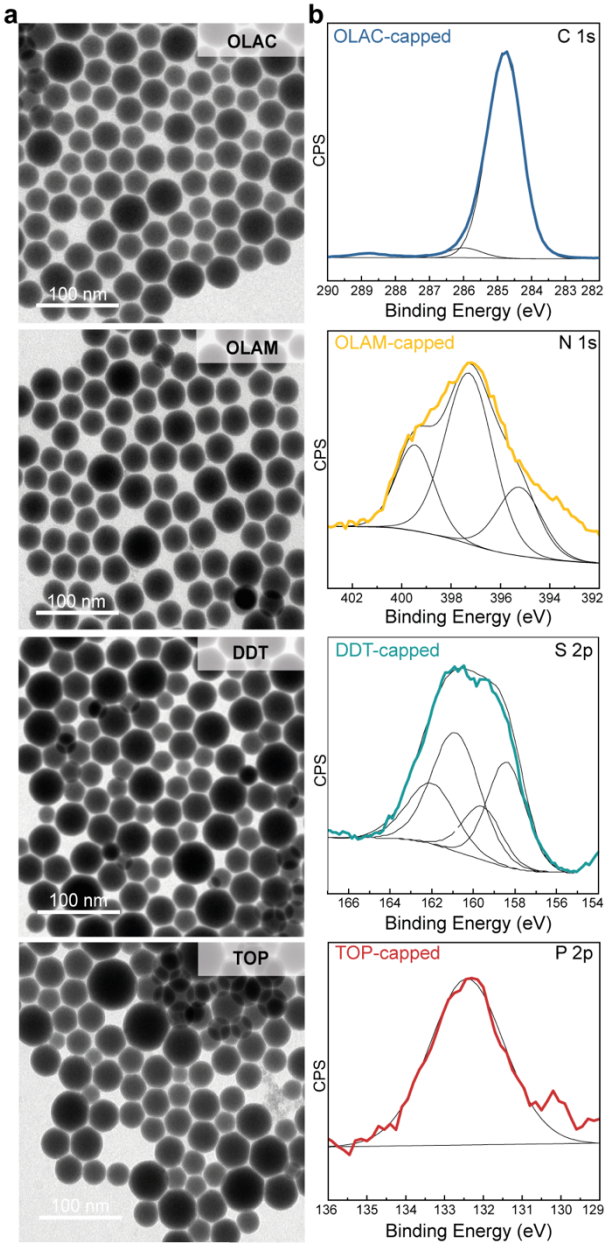

Figure 1. (a) TEM images of the as-synthesized Ga NPs with different ligands; (b) XPS spectra for -C, -N, -P and -S indicating the presence of the ligands on the surface. The peak at 288.72 eV in the C1s spectrum for the OLAC-capped sample is assigned to carboxylic carbon (COOH).

To gain insight into the effect of the different capping agents on the oxide skin, we used XPS complemented with electron microscopy techniques. The samples were characterized just after their synthesis and particular care was taken in the transfer from the glove box to the instrument. **Figure 2** reports a summary of the obtained results. The complete data set and a detailed explanation of their interpretation is reported in the **Supporting Information** (**Figures S3, S4**).

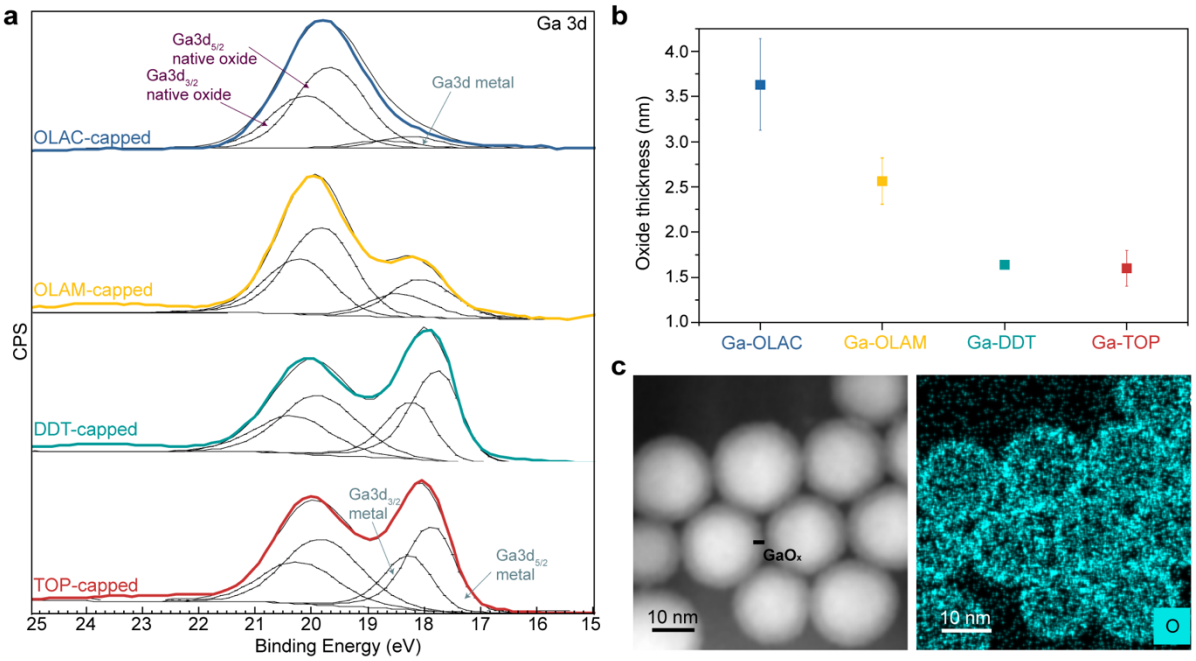

Figure 2. (a) XPS spectra of the Ga 3d region for the as-synthesized ligand-capped NPs, evidencing the simultaneous presence of Ga metal and Ga oxide with different ratios in each case; (b) oxide thickness, with corresponding error bars, calculated from the XPS data for the different ligands (note that the error bar for DDT is too small to be seen); (c) STEM-HAADF image (left) and corresponding EDXS elemental map (right) of OLAM-capped Ga NPs showing the presence of an oxide shell as a lighter contrast (left) and in blue (right). The measured oxide thickness on the STEM-HAADF image corresponds to 2.6 nm, matching well with the XPS calculation reported in (b).

Similarly to other reports,[25,26,36] the XPS spectra were fitted with two peaks in the Ga 3d region for each sample (**Figure 2a**). The peak at around 20 eV corresponds to gallium oxide whereas the peak at around 18 eV can be assigned to metallic Ga. The relative ratio of these two peaks changes across the samples indicating differences in the oxide-to-metal contribution. The thickness of the oxide, which can be approximated from this ratio (details in the **Supporting Information**), decreases from around 3.5 nm to 1.5 nm following the trend OLAC>OLAM>DDT~TOP (**Figure 2b**). High-angle annular dark-field scanning TEM (HAADF-STEM) imaging and energy dispersive X-ray spectroscopy (EDXS) corroborate the thickness of around 2.6 nm for the OLAM-capped NPs (**Figure 2c**). Therefore, we can

confidently compare the extent of the oxidation between the four samples: OLAC-capped particles have the thickest oxide shell followed by OLAM-, DDT- and TOP-capped Ga NPs, with the latter two being approximately equal.

To understand the observed trend, we investigated the oxide evolution over time. Our aim was to elucidate the interplay between kinetics (i.e., delayed oxidation) and thermodynamics (i.e., thinner final oxide thicknesses under equilibrium conditions). To reach the equilibrium conditions, we left samples deposited as thin films exposed to air for five days. No further changes were observed in samples left for over one month under the same conditions. **Figure 3** summarizes the obtained data. The XPS spectra of the samples can still be deconvoluted into the gallium oxide and metallic Ga peaks, although the contribution of the former increases compared to the as-synthesized samples (**Figure 3a**). This trend becomes more evident when plotting the oxide thicknesses for the ligand-functionalized Ga NPs (**Figure 3b**). When compared to the measurement on day zero, OLAC ended up with the thickest shell, which decreased with OLAM>DDT>TOP, with the latter clearly presenting the thinnest shell-(**Figure 3b,c**).

The observation that the NPs do not become fully oxidized and preserve a metallic core even when exposed to air for several days is consistent with the self-passivating nature of the gallium oxide skin. This behavior can be interpreted via the well-established Cabrera-Mott theory.[37–39] According to this theory, oxygen chemisorption quickly initiates the formation of a monolayer of gallium oxide. However, electrons can still pass from the core through the oxide and ionize adsorbed O_2.[26] The formation of negatively charged oxygen ions on the surface and positively charged metal ions in the core generates an electric field (the Mott potential, V_M) , which drives the oxide formation. If the diffusion coefficient of the metal ions through the oxide layer is larger than that of the oxygen ions, then voids in the metal core form (Kirkendall effect).[40,41]

In the case of Ga, the oxide growth rate follows a logarithmic trend and ends when a critical thickness is reached, generally up to a few weeks.[25,42–44] This passivating effect of the oxide layer prevents the metal from further oxidation. In the case of NPs, the higher surface-to-volume ratio is expected to accelerate the oxide growth compared to bulk materials.[38] Indeed, we found that samples stored in solution and under inert atmosphere for five days possessed a very similar oxide thickness to the samples exposed to air (**Figure S6**). This observation demonstrates that the oxidation rate is relatively fast even with extremely low concentrations of adventitious oxygen.

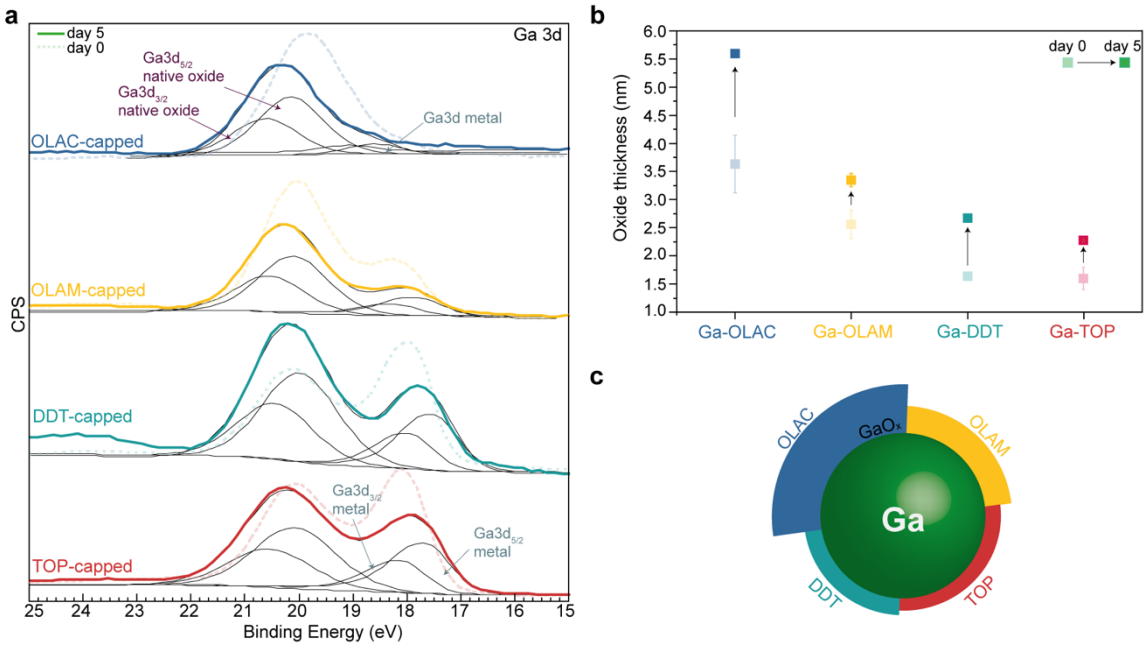

Figure 3. (a) XPS spectra of the Ga 3d region for the ligand-capped NPs that were aged for 5 days in air; the as-synthesized Ga NP spectra are also shown as a reference (dashed); (b) oxide thicknesses with corresponding error bars for the "aged" ligand-capped Ga NPs. Note that no error could be calculated for the aged OLAC-capped sample because no signal for Ga metal could be found in the Ga 2p spectra (see **Figure S2** and more details in the Supporting Information) and that the errors for TOP and DDT are too small to be seen; (c) sketch representing the oxide thickness for each ligand.

To understand the changing influence of the ligands on the oxide thickness with time, different factors must be considered. We assume that a combination of thermodynamics and kinetics

dominate at day 0 while thermodynamics will be more important at day 5 and after that. From a thermodynamic point of view, the aforementioned ligand's binding preference towards the metal or the metal oxide is certainly an important parameter.[32–35,45] However, the ligand's dipole moment and subsequent effect on the V_M should also be considered.[25,46–49] From a purely kinetic perspective, the packing density on the surface should be taken into account as it can alter the oxygen accessibility to surface sites.[25–27,50,51]

To comprehend the observed trends, let us discuss each group separately starting with OLAC and OLAM. Hens et al. have previously empirically demonstrated that both amines and carboxylic acids (in the form of carboxylates), bind to Cu NPs through surface oxide sites.[32] Both ligands have the same alkyl chain and only differ in their functional group. Hence, it is reasonable to think that they would pack similarly on the surface of Ga NPs without imparting big differences on the availability of surface sites, i.e., kinetics, for the oxide growth. On the other hand, according to the HSAB theory, carboxylates are harder bases than amines and thus have a higher affinity toward hard acids, like Ga^{3+}.[34,45] Therefore, OLAC simultaneously favors the outgoing diffusion of Ga^{3+} ions during the oxide formation and passivates the oxide better, eventually promoting the formation of a thicker shell than OLAM.

The comparison between TOP and DDT is less straightforward since both their alkyl chains and functional groups are different (we note that these ligands are not commercially available or even stable with the same chain length and their synthesis is not trivial). Thiols and phosphines are soft bases with greater affinity towards soft acids, which explains why they are suitable ligands if one wants to hinder the oxidation of Ga NPs. Phosphines are softer bases than thiols and, as a result, have an even stronger affinity for metal sites.

In addition to the HSAB theory, TOP has a larger electric dipole moment (>>1.2 D) than DDT (~0.8 D) and so it is expected to oppose the V_M to a greater extent, ultimately reducing the final oxide thickness. Overall, thermodynamics point towards a thicker oxide shell for DDT than for TOP, which is indeed what we observe after 5 days (**Figure 4**).

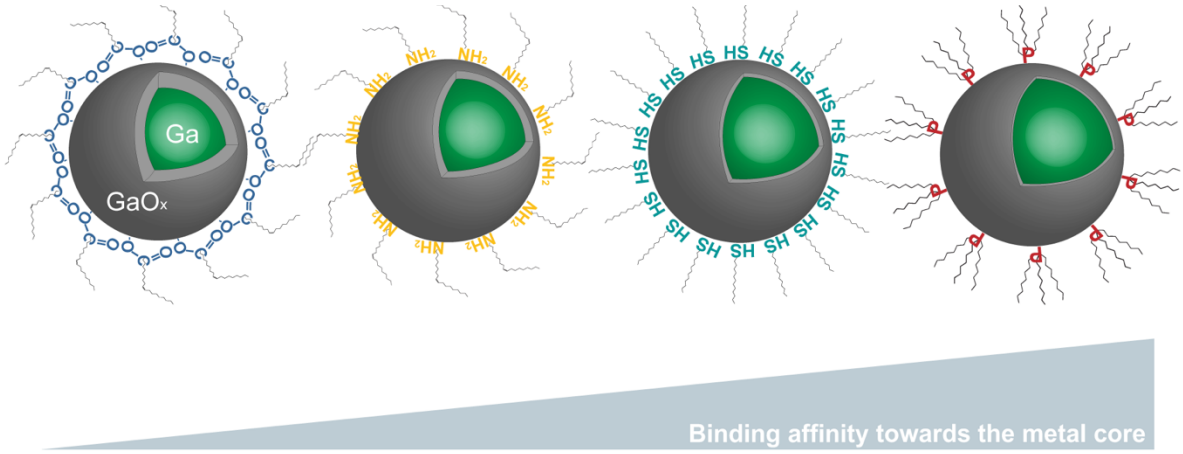

Figure 4. Schematic representation illustrating how different ligands affect the native gallium oxide shell thickness and the main parameter governing thermodynamic oxide tunability using ligands.

On the other hand, DDT's saturated single carbon chain is prone to create dense self-assembled monolayers (SAMs) on metallic NP surfaces.[25–27,35,52,53] In contrast, the bulkier TOP ligand will form a less compact SAM, which results in less impediment of the oxygen diffusion towards the Ga surface. Nevertheless, DDT-capped and TOP-capped Ga NPs display similar oxide thickness at day 0. Only the combination of the opposing thermodynamics and kinetics effect can justify this result. A similar argument was used by Tabor et al. when comparing the effect of thiols with different substitution and dipole moments on the oxide growth of a mixture of nano- and micron-sized eutectic GaIn particles.[25]

Having assessed the impact that these different ligands have on the oxidation of colloidal Ga NPs, we decided to investigate its effect on their chemical reactivity. The self-passivating oxide shell is known to impact the chemical and mechanical behavior of liquid metals.[2-4,16,18,31,43–48]

The oxide shell was recently discovered to strongly influence the behavior of Ga NPs in the galvanic replacement reaction (GRR).[31] In particular, OLAC-capped Ga NPs were found to react with a copper amine complex to form Cu-Ga nanodimers.[31] This morphology was explained by the presence of the oxide shell preventing the Cu-Ga alloying. Therefore, we explored the same reaction with OLAM-, DDT- and TOP-capped Ga NPs, possessing decreasing oxide thicknesses, and using the OLAC-capped NPs as a control.

Figure 5 summarizes the obtained results. Interestingly, we can separate the products into two categories according to their morphologies (**Figure 5a** and **Figure 5b**). The OLAC- and OLAM-capped Ga NPs form Cu-Ga nanodimers, similarly to previous results.[31] Indeed, the bright-field TEM images (**Figure 5c,d**) indicate that the lower contrast Ga domain possesses a smaller size than the starting NPs, as well as a deformed shape (**Table S1**), which narrows towards the interface with the crystalline Cu domain. Conversely, homogeneous nucleation of crystalline Cu NPs, separated from the amorphous Ga domains, is observed with the TOP- and DDT-capped Ga NPs (**Figure 5e,f**).

These differences are even more evident in the STEM-HAADF and EDX images (**Figures 5g,h** and **5i,j)**. The white arrow in **Figure 5g** points to the presence of a lower contrast interface between the Cu and the Ga domains, which corresponds to the gallium oxide shell. As described in the previously cited work,[31] this interface causes the deformation of the Ga domain. On the other hand, **Figure 5i,j** shows that Ga and Cu NPs are physically mixed and do not share an interface.

These results suggest that the oxide thickness determines in what fashion the GRR proceeds. GRRs are electrochemical processes in which a sacrificial metal (in our case Ga^0 in the NP core) is oxidized by a metal cation in solution possessing a more positive redox potential (in

our case Cu^{2+}) that, in turn, gets reduced and deposits onto the pre-existing template.[31,56–62] Examples in the literature indicate that capping ligands can influence the deposition by modifying the surface properties or acting as co-reducing agents.[61,63,64] Therefore, to be conclusive regarding the role of the oxide, we performed a series of control experiments in which we carried out a ligand exchange between OLAC-capped Ga NPs and OLAM, DDT and TOP after the oxide shell had already formed. By doing so, we expected to maintain a thick gallium oxide shell that was independent of the capping ligand, hence keeping one of the parameters of study constant (see **Supporting Information** and **Figures S7-S9**). After each GRR, Cu-Ga nanodimers formed independently of the capping ligand (**Figure S8**). Thus, we can establish that the heterogenous versus homogeneous nucleation of Cu solely depends on the gallium oxide thickness of the Ga NPs which, in turn, depends on the initial ligands capping their surface.

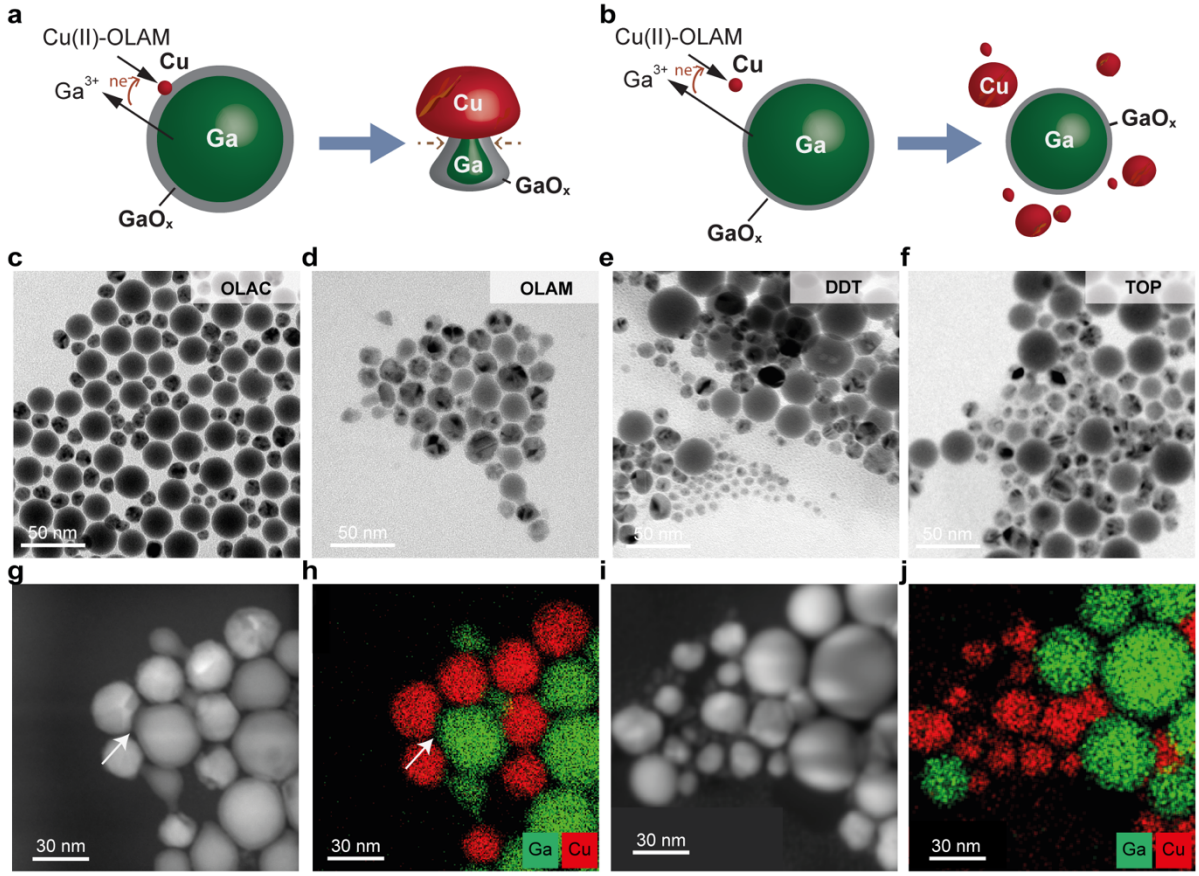

Figure 5. Sketch of the proposed reaction mechanism for (a) OLAC- and OLAM- and (b) for DDT- and TOP-capped Ga NPs with the Cu precursor; TEM images of the resulting NPs after GRR with (c) OLAC- and (d) OLAM-capped Ga NPs show the formation of Cu-Ga nanodimers, as confirmed by (g) STEM-HAADF and (h) EDX of the OLAM-capped samples; on the other hand, when (e) DDT and (f) TOP are used, the GRR results in separate Cu and Ga NPs as evidenced by their corresponding TEM images and (i) STEM-HAADF and (j) EDX of the DDT-capped samples.

Having confidently concluded that the oxide shell thickness determines the outcome of the GRR, qualitative information on the reaction rate can be derived from the analysis of the size evolution of the Ga and Cu domains along with the relative concentration between the two metals in the final reaction product (**Table S1**). These data indicate that OLAM-capped Ga NPs undergo a faster GRR than OLAC-capped ones, which is consistent with a thinner oxide shell facilitating the migration of Ga atoms from the NP core into the solution. In the case of the TOP- and DDT-capped Ga NPs, the size and elemental analyses indicate that a GRR still

takes place, though at a lower extent than expected based on a thinner oxide shell. This puzzling result prompts a final question: why does the thinner oxide shell in DDT- and TOP-capped Ga NPs not facilitate the outward diffusion of Ga and promote a separate nucleation of Cu? First of all, we note that the amorphous Ga oxide skin possesses a very complex layered structure that makes it unique compared to other oxides, like alumina.[16,65] We hypothesize that this feature prevents the transport of copper atoms and, thus, their alloying with gallium. Moreover, thicker oxide shells are expected to have a higher degree of short range structural order.[43,66–69] The latter can reduce the nucleation energy barrier of a new crystalline phase, in this case copper. Conversely, a thinner oxide would show a more liquid-like behavior[18,70] that eventually prevents heterogeneous nucleation of an ordered phase. Since homogeneous nucleation is energetically more expensive, Cu nucleation, and hence Ga outwards diffusion, would occur at a slower rate than if heterogeneous nucleation took place under the same conditions. Here, future in-depth characterization, including high resolution microscopy and pair distribution function analysis, will be pursued to verify these hypotheses and to further comprehend the complex structure and properties of gallium oxide on Ga NPs.

CONCLUSIONS

In conclusion, we have demonstrated the modulating effect of capping ligands on the surface oxidation of liquid Ga NPs and the importance of the oxide shell thickness on the reactivity of Ga NPs in the framework of the GRR. A thorough analysis of the surface of these Ga NPs has revealed that DDT and TOP are the most suitable ligands if the aim is to hinder the gallium oxide growth. On the other hand, OLAM and, in particular, OLAC are less efficient in moderating the oxidation of the Ga surface. Nevertheless, none of the ligands were able to completely supress the oxidation of Ga even when working under inert conditions.

Through a number of systematic experiments, we have evidenced how the oxide thickness governs the nucleation fashion of a Cu precursor during a GRR with Ga. Thicker oxide shells promote the heterogenous nucleation of Cu to form Cu-Ga nanodimers; contrariwise, thinner shells lead to a separated nucleation of Cu particles.

Overall, we showcase the importance of ligands when studying Ga NPs as well as the unique behavior of these nanomaterials and the need for further exploration of their chemistry. We also highlight that in all Ga-based LM alloys, the oxide skin still consists of gallium oxide, therefore these findings are expected to be of interest to a wider community.

Given the increasing number of original publications and reviews[2–4,16,22,30,42,71] on the applications and fundamentals of Ga-based micro- and nano-particles, this work aims to serve as a reference for future studies in several disciplines.

ASSOCIATED CONTENT

The Supporting Information is available and free of charge and contains additional experimental details, information related to XPS experiments and additional XPS data, TEM results and discussions.

ACKNOWLEDGEMENTS

This work was primarily financed by the Swiss National Science Foundation (SNSF) under the grant nº 200021L_191997/1. JRP is supported by the H2020 Marie Curie Individual Fellowship grant SURFCAT with agreement number 837378. The authors thank Dr. Mounir

Mensi for the help with the XPS data analysis. Valery Okatenko and Dr Anna Loiudice are acknowledged for helpful discussions on the nature of the gallium oxide shell and critical reading of the manuscript, respectively.

TOC:

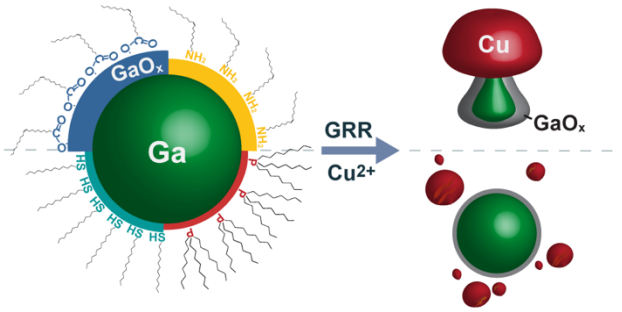

REFERENCES

(1) Zhang, W.; Ou, J. Z.; Tang, S. Y.; Sivan, V.; Yao, D. D.; Latham, K.; Khoshmanesh, K.; Mitchell, A.; O'Mullane, A. P.; Kalantar-Zadeh, K. Liquid Metal/Metal Oxide Frameworks. *Adv. Funct. Mater.* **2014**, *24*, 3799–3807.

(2) Daeneke, T.; Khoshmanesh, K.; Mahmood, N.; De Castro, I. A.; Esrafilzadeh, D.; Barrow, S. J.; Dickey, M. D.; Kalantar-Zadeh, K. Liquid Metals: Fundamentals and Applications in Chemistry. *Chem. Soc. Rev.* **2018**, *47*, 4073–4111.

(3) Song, H.; Kim, T.; Kang, S.; Jin, H.; Lee, K.; Yoon, H. J. Ga-Based Liquid Metal Micro/Nanoparticles: Recent Advances and Applications. *Small* **2019**, *1903391*, 1–21.

(4) Kalantar-Zadeh, K.; Tang, J.; Daeneke, T.; O'Mullane, A. P.; Stewart, L. A.; Liu, J.; Majidi, C.; Ruoff, R. S.; Weiss, P. S.; Dickey, M. D. Emergence of Liquid Metals in Nanotechnology. *ACS Nano* **2019**, *13*, 7388–7395.

(5) Bo, G.; Yu, H.; Ren, L.; Cheng, N.; Feng, H.; Xu, X.; Xue Dou, S.; Wang, H.; Du, Y. Gallium–Indium–Tin Liquid Metal Nanodroplet-Based Anisotropic Conductive Adhesives for Flexible Integrated Electronics. *ACS Appl. Nano Mater.* **2021**, *4*, 550–557.

(6) Wan, A.; Suchand Sangeeth, C. S.; Wang, L.; Yuan, L.; Jiang, L.; Nijhuis, C. A. Arrays of High Quality SAM-Based Junctions and Their Application in Molecular Diode Based Logic. *Nanoscale* **2015**, *7*, 19547–19556.

(7) Sun, X.; Yuan, B.; Sheng, L.; Rao, W.; Liu, J. Liquid Metal Enabled Injectable Biomedical Technologies and Applications. *Appl. Mater. Today* **2020**, *20*, 100722.

(8) Lu, Y.; Hu, Q.; Lin, Y.; Pacardo, D. B.; Wang, C.; Sun, W.; Ligler, F. S.; Dickey, M. D.; Gu, Z. Transformable Liquid-Metal Nanomedicine. *Nat. Commun.* **2015**, *6*, 1–10.

(9) Sun, X.; Sun, M.; Liu, M.; Yuan, B.; Gao, W.; Rao, W.; Liu, J. Shape Tunable Gallium Nanorods Mediated Tumor Enhanced Ablation through Near-Infrared Photothermal Therapy. *Nanoscale* **2019**, *11*, 2655–2667.

(10) Chechetka, S. A.; Yu, Y.; Zhen, X.; Pramanik, M.; Pu, K.; Miyako, E. Light-Driven Liquid Metal Nanotransformers for Biomedical Theranostics. *Nat. Commun.* **2017**, *8*, 1–19.

(11) Yarema, M.; Wörle, M.; D. Rossell, M.; Erni, R.; Caputo, R.; Protesescu, L.; V. Kravchyk, K.; N. Dirin, D.; Lienau, K.; von Rohr, F.; et al. Monodisperse Colloidal Gallium Nanoparticles: Synthesis, Low Temperature Crystallization, Surface Plasmon Resonance and Li-Ion Storage. *J. Am. Chem. Soc.* **2014**, *136*, 12422–12430.

(12) Esrafilzadeh, D.; Zavabeti, A.; Jalili, R.; Atkin, P.; Choi, J.; Carey, B. J.; Brkljača, R.; O'Mullane, A. P.; Dickey, M. D.; Officer, D. L.; et al. Room Temperature CO2 Reduction to Solid Carbon Species on Liquid Metals Featuring Atomically Thin Ceria Interfaces. *Nat. Commun.* **2019**, *10*.

(13) Taccardi, N.; Grabau, M.; Debuschewitz, J.; Distaso, M.; Brandl, M.; Hock, R.; Maier, F.; Papp, C.; Erhard, J.; Neiss, C.; et al. Gallium-Rich Pd-Ga Phases as Supported Liquid Metal Catalysts. *Nat. Chem.* **2017**, *9*, 862–867.

(14) Liu, H.; Xia, J.; Zhang, N.; Cheng, H.; Bi, W.; Zu, X.; Chu, W.; Wu, H.; Wu, C.; Xie, Y. Solid–Liquid Phase Transition Induced Electrocatalytic Switching from Hydrogen Evolution to Highly Selective CO2 Reduction. *Nat. Catal.* **2021**, *4*, 202–211.

(15) Knight, M. W.; Coenen, T.; Yang, Y.; Brenny, B. J. M.; Losurdo, M.; Brown, A. S.; Everitt, H. O.; Polman, A. Gallium Plasmonics: Deep Subwavelength Spectroscopic Imaging of Single and Interacting Gallium Nanoparticles. *ACS Nano* **2015**, *9*, 2049–2060.

(16) Martin, A.; Du, C.; Chang, B.; Thuo, M. Complexity and Opportunities in Liquid Metal Surface Oxides. *Chem. Mater.* **2020**, *32*, 9045–9055.

(17) Doudrick, K.; Liu, S.; Mutunga, E. M.; Klein, K. L.; Damle, V.; Varanasi, K. K.; Rykaczewski, K. Different Shades of Oxide: From Nanoscale Wetting Mechanisms to Contact Printing of Gallium-Based Liquid Metals. *Langmuir* **2014**, *30*, 6867–6877.

(18) Kim, D.; Thissen, P.; Viner, G.; Lee, D. W.; Choi, W.; Chabal, Y. J.; Lee, J. B. Recovery of Nonwetting Characteristics by Surface Modification of Gallium-Based Liquid Metal Droplets Using Hydrochloric Acid Vapor. *ACS Appl. Mater. Interfaces* **2013**, *5*, 179–185.

(19) Khan, M. R.; Eaker, C. B.; Bowden, E. F.; Dickey, M. D. Giant and Switchable Surface Activity of Liquid Metal via Surface Oxidation. *Proc. Natl. Acad. Sci. U. S. A.* **2014**, *111*, 14047–14051.

(20) Kramer, R. K.; Boley, J. W.; Stone, H. A.; Weaver, J. C.; Wood, R. J. Effect of Microtextured Surface Topography on the Wetting Behavior of Eutectic Gallium-Indium Alloys. *Langmuir* **2014**, *30*, 533–539.

(21) Wissman, J.; Dickey, M. D.; Majidi, C. Field-Controlled Electrical Switch with Liquid Metal. *Adv. Sci.* **2017**, *4*.

(22) Liu, S.; Sweatman, K.; McDonald, S.; Nogita, K. Ga-Based Alloys in Microelectronic Interconnects: A Review. *Materials (Basel).* **2018**, *11*, 1–20.

(23) Tabor, C.; Holcomb, S.; Heikenfeld, J. Reliable and Reversible Contact of Eutectic

Gallium Indium and Copper Electrodes. *Adv. Mater. Interfaces* **2020**, *7*, 1–8.

(24) Martin, A.; Chang, B. S.; Pauls, A. M.; Du, C.; Thuo, M. Stabilization of Undercooled Metals via Passivating Oxide Layers. *Angew. Chemie* **2021**, *133*, 5993–6000.

(25) Farrell, Z. J.; Tabor, C. Control of Gallium Oxide Growth on Liquid Metal Eutectic Gallium/Indium Nanoparticles via Thiolation. *Langmuir* **2018**, *34*, 234–240.

(26) Morris, N. J.; Farrell, Z. J.; Tabor, C. E. Chemically Modifying the Mechanical Properties of Core-Shell Liquid Metal Nanoparticles. *Nanoscale* **2019**, *11*, 17308–17318.

(27) Hohman, J. N.; Kim, M.; Wadsworth, G. A.; Bednar, H. R.; Jiang, J.; Lethai, M. A.; Weiss, P. S. Directing Substrate Morphology via Self-Assembly: Ligand-Mediated Scission of Gallium-Indium Microspheres to the Nanoscale. *Nano Lett.* **2011**, *11*, 5104–5110.

(28) Tevis, I. D.; Newcomb, L. B.; Thuo, M. Synthesis of Liquid Core-Shell Particles and Solid Patchy Multicomponent Particles by Shearing Liquids into Complex Particles (SLICE). *Langmuir* **2014**, *30*, 14308–14313.

(29) Han, J.; Tang, J.; Idrus-Saidi, S. A.; Christoe, M. J.; O'Mullane, A. P.; Kalantar-Zadeh, K. Exploring Electrochemical Extrusion of Wires from Liquid Metals. *ACS Appl. Mater. Interfaces* **2020**, *12*, 31010–31020.

(30) Dickey, M. D. Emerging Applications of Liquid Metals Featuring Surface Oxides. *ACS Appl. Mater. Interfaces* **2014**, *6*, 18369–18379.

(31) Castilla-Amorós, L.; Stoian, D.; Pankhurst, J. R.; Varandili, S. B.; Buonsanti, R. Exploring the Chemical Reactivity of Gallium Liquid Metal Nanoparticles in Galvanic Replacement. *J. Am. Chem. Soc.* **2020**, *142*, 19283–19290.

(32) Oliva-Puigdomènech, A.; De Roo, J.; Kuhs, J.; Detavernier, C.; Martins, J. C.; Hens, Z. Ligand Binding to Copper Nanocrystals: Amines and Carboxylic Acids and the Role of Surface Oxides. *Chem. Mater.* **2019**, *31*, 2058–2067.

(33) Dabera, G. Di. M. R.; Walker, M.; Sanchez, A. M.; Pereira, H. J.; Beanland, R.; Hatton, R. A. Retarding Oxidation of Copper Nanoparticles without Electrical Isolation and the Size Dependence of Work Function. *Nat. Commun.* **2017**, *8*.

(34) Pearson, R. G. Hard and Soft Acids and Bases. *J. Am. Chem. Soc.* **1963**, *85*, 3533–3539.

(35) Heuer-Jungemann, A.; Feliu, N.; Bakaimi, I.; Hamaly, M.; Alkilany, A.; Chakraborty, I.; Masood, A.; Casula, M. F.; Kostopoulou, A.; Oh, E.; et al. The Role of Ligands in the Chemical Synthesis and Applications of Inorganic Nanoparticles. *Chem. Rev.* **2019**, *119*, 4819–4880.

(36) Cademartiri, L.; Thuo, M. M.; Nijhuis, C. A.; Reus, W. F.; Tricard, S.; Barber, J. R.; Sodhi, R. N. S.; Brodersen, P.; Kim, C.; Chiechi, R. C.; et al. Electrical Resistance of Ag ... Tunnerling Junctions. *J. Phys. Chem. C* **2012**, No. 116, 10848–10860.

(37) Cabrera, N. .; Mott, N. F. Theory of the Oxidation of Metals. *Reports Prog. Phys.* **1949**, *12*, 163.

(38) Zhdanov, V. P.; Kasemo, B. Cabrera-Mott Kinetics of Oxidation of Nm-Sized Metal Particles. *Chem. Phys. Lett.* **2008**, *452*, 285–288.

(39) Ermoline, A.; Dreizin, E. L. Equations for the Cabrera-Mott Kinetics of Oxidation for Spherical Nanoparticles. *Chem. Phys. Lett.* **2011**, *505*, 47–50.

(40) Kirkendall, E. O. Diffusion Of Zinc in Alpha Brass. *Trans. AIME* **1942**, *171*, 104–110.

(41) Zhdanov, V. P. Kinetic Model of Oxidation of Metal Nanoparticles: Cabrera-Mott and Kirkendall Effects. *Surf. Sci.* **2019**, *684*, 24–27.

(42) Lin, Y.; Genzer, J.; Dickey, M. D. Attributes, Fabrication, and Applications of Gallium-Based Liquid Metal Particles. *Adv. Sci.* **2020**, *7*.

(43) Regan, M.; Tostmann, H.; Pershan, P.; Magnussen, O.; DiMasi, E.; Ocko, B. X-Ray Study of the Oxidation of Liquid-Gallium Surfaces. *Phys. Rev. B - Condens. Matter Mater. Phys.* **1997**, *55*, 10786–10790.

(44) Sutter, E.; Sutter, P. Size-Dependent Room Temperature Oxidation of in Nanoparticles. *J. Phys. Chem. C* **2012**, *116*, 20574–20578.

(45) Pearson, R. G. Acids and Bases. *Science.* **1966**, *151*, 172–177.

(46) Schmidt, C.; Witt, A.; Witte, G. Tailoring the Cu(100) Work Function by Substituted Benzenethiolate Self-Assembled Monolayers. *J. Phys. Chem. A* **2011**, *115*, 7234–7241.

(47) Otálvaro, D.; Veening, T.; Brocks, G. Self-Assembled Monolayer Induced Au(111) and Ag(111) Reconstructions: Work Functions and Interface Dipole Formation. *J. Phys. Chem. C* **2012**, *116*, 7826–7837.

(48) Wu, K. Y.; Yu, S. Y.; Tao, Y. T. Continuous Modulation of Electrode Work Function with Mixed Self-Assembled Monolayers and Its Effect in Charge Injection. *Langmuir* **2009**, *25*, 6232–6238.

(49) Rusu, P. C.; Brocks, G. Surface Dipoles and Work Functions of Alkylthiolates and Fluorinated Alkylthiolates on Au(111). *J. Phys. Chem. B* **2006**, *110*, 22628–22634.

(50) Zhdanov, V. P.; Norton, P. R. Kinetics of Thin Oxide Film Growth on Metal Crystals. *Surf. Rev. Lett.* **2000**, *7*, 135–139.

(51) Itoh, M.; Nishihara, H.; Aramaki, K. The Protection Ability of 11-Mercapto-1-undecanol Self-Assembled Monolayer Modified with Alkyltrichlorosilanes Against

Corrosion of Copper. *J. Electrochem. Soc.* **1995**, *142*, 1839–1846.

(52) Kanninen, P.; Johans, C.; Merta, J.; Kontturi, K. Influence of Ligand Structure on the Stability and Oxidation of Copper Nanoparticles. *J. Colloid Interface Sci.* **2008**, *318*, 88–95.

(53) Inkpen, M. S.; Liu, Z. –F; Li, H.; Campos, L. M.; Neaton, J. B.; Venkataraman, L. Non-Chemisorbed Gold–Sulfur Binding Prevails in Self-Assembled Monolayers. *Nat. Chem.* **2019**, *11*, 351–358.

(54) Ladd, C.; So, J. H.; Muth, J.; Dickey, M. D. 3D Printing of Free Standing Liquid Metal Microstructures. *Adv. Mater.* **2013**, *25*, 5081–5085.

(55) Zavabeti, A.; Ou, J. Z.; Carey, B. J.; Syed, N.; Orrell-Trigg, R.; Mayes, E. L. H.; Xu, C.; Kavehei, O.; O'Mullane, A. P.; Kaner, R. B.; et al. A Liquid Metal Reaction Environment for the Room-Temperature Synthesis of Atomically Thin Metal Oxides. *Science.* **2017**, *358*, 332–335.

(56) Xia, X.; Wang, Y.; Ruditskiy, A.; Xia, Y. 25th Anniversary Article: Galvanic Replacement: A Simple and Versatile Route to Hollow Nanostructures with Tunable and Well-Controlled Properties. *Adv. Mater.* **2013**, *25*, 6313–6332.

(57) Sun, Y.; T. Mayers, B.; Xia, Y. Template-Engaged Replacement Reaction: A One-Step Approach to the Large-Scale Synthesis of Metal Nanostructures with Hollow Interiors. *Nano Lett.* **2002**, *2*, 481–485.

(58) Yang, Y.; Zhang, Q.; Fu, Z. W.; Qin, D. Transformation of Ag Nanocubes into Ag-Au Hollow Nanostructures with Enriched Ag Contents to Improve SERS Activity and Chemical Stability. *ACS Appl. Mater. Interfaces* **2014**, *6*, 3750–3757.

(59) Chen, A. N.; McClain, S. M.; House, S. D.; Yang, J. C.; Skrabalak, S. E. Mechanistic Study of Galvanic Replacement of Chemically Heterogeneous Templates. *Chem. Mater.* **2019**, *31*, 1344–1351.

(60) Oh, M. H.; Yu, T.; Yu, S.-H.; Lim, B.; Ko, K.-T.; Willinger, M.-G.; Seo, D.-H.; Kim, B. H.; Cho, M. G.; Park, J.-H.; et al. Galvanic Replacement Reactions in Metal Oxide Nanocrystals. *Science.* **2013**, *340*, 964–969.

(61) Da Silva, A. G. M.; Rodrigues, T. S.; Haigh, S. J.; Camargo, P. H. C. Galvanic Replacement Reaction: Recent Developments for Engineering Metal Nanostructures towards Catalytic Applications. *Chem. Commun.* **2017**, *53*, 7135–7148.

(62) Hoshyargar, F.; Crawford, J.; O'Mullane, A. P. Galvanic Replacement of the Liquid Metal Galinstan. *J. Am. Chem. Soc.* **2017**, *139*, 1464–1471.

(63) Jing, H.; Wang, H. Structural Evolution of Ag-Pd Bimetallic Nanoparticles through

Controlled Galvanic Replacement: Effects of Mild Reducing Agents. *Chem. Mater.* **2015**, *27*, 2172–2180.

(64) Polavarapu, L.; Zanaga, D.; Altantzis, T.; Rodal-Cedeira, S.; Pastoriza-Santos, I.; Pérez-Juste, J.; Bals, S.; Liz-Marzán, L. M. Galvanic Replacement Coupled to Seeded Growth as a Route for Shape-Controlled Synthesis of Plasmonic Nanorattles. *J. Am. Chem. Soc.* **2016**, *138*, 11453–11456.

(65) Коршунов, В. Поведение Вращающегося Дискового Ga-Анода в Щелочной Среде. *Электрохимия* **1995**, *31*, 1122.

(66) Lan, S.; Zhu, L.; Wu, Z.; Gu, L.; Zhang, Q.; Kong, H.; Liu, J.; Song, R.; Liu, S.; Sha, G.; et al. A Medium-Range Structure Motif Linking Amorphous and Crystalline States. *Nat. Mater.* **2021**.

(67) Elliott, S. R. Medium-Range Structural Order in Covalent Amorphous Solids. *Nature* **1991**, *354*, 445–452.

(68) Regan, M. J.; Kawamoto, E. H.; Lee, S.; Pershan, P. S.; Maskil, N.; Deutsch, M.; Magnussen, O. M.; Ocko, B. M.; Berman, L. E. Surface Layering in Liquid Gallium: An x-Ray Reflectivity Study. *Phys. Rev. Lett.* **1995**, *75*, 2498–2501.

(69) Yagafarov, O. F.; Katayama, Y.; Brazhkin, V. V.; Lyapin, A. G.; Saitoh, H. Energy Dispersive X-Ray Diffraction and Reverse Monte Carlo Structural Study of Liquid Gallium under Pressure. *Phys. Rev. B - Condens. Matter Mater. Phys.* **2012**, *86*, 1–9.

(70) Khondoker, M. A. H.; Sameoto, D. Fabrication Methods and Applications of Microstructured Gallium Based Liquid Metal Alloys. *Smart Mater. Struct.* **2016**, *25*.

(71) Dickey, M. D. Liquid Metals at Room Temperature. *Physics Today*. American Institute of Physics 2021, pp 30–36.